CRYSTAL GROWTH & DESIGN

pubs.acs.org/crystal

Article

Effects of Fe Deficiency and Co Substitution in Polycrystalline and Single Crystals of Fe_3GeTe_2

Daniel A. Mayoh,* George D. A. Wood, Samuel J. R. Holt, Grady Beckett, Emily J. L. Dekker, Martin R. Lees, and Geetha Balakrishnan*

Cite This: https://doi.org/10.1021/acs.cgd.1c00684

Read Online

ACCESS | Metrics & More | Article Recommendations

ABSTRACT: Fe_3GeTe_2 is a two-dimensional van der Waals material with a ferromagnetic ground state and a maximum transition temperature $T_c \sim 225$ K. However, when Fe_3GeTe_2 is synthesized, lower values of T_c are often reported. This is attributed to a deficiency in the Fe at the 2c site in the crystal structure. Here, we investigate the effect of Fe deficiency and the substitution of Co for Fe on the magnetic properties of this system. We have synthesized both polycrystalline material and single crystals by chemical vapor transport and the flux method, with the largest crystals obtained using the flux method. Cobalt substitution at the Fe site is found to significantly reduce the magnetic transition temperature. Crystals of Fe_3GeTe_2 grown by chemical vapor transport with ~ 8% excess Fe in the starting materials display an optimum Fe content and magnetic transition temperature.

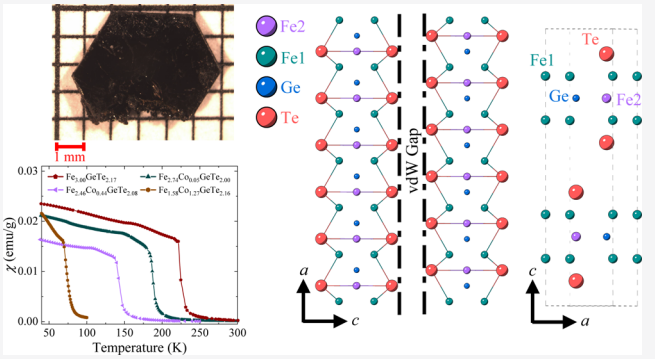

INTRODUCTION

Van der Waals (vdW) bonded magnetic materials are currently shaping the field of two-dimensional (2D) materials science.[1] The presence of van der Waals bonding in these materials allows them to be cleaved down to monolayers and combined with other 2D materials to create novel heterostructures without concern for lattice matching. By modifying these heterostructures, the electrical, optical, and magnetic properties can be fine-tuned, and in some cases, unique magnetic phases can be realized.[2] Many magnetic vdW materials have been discovered to host an assortment of magnetic orders such as ferromagnetism (e.g., CrB_3,[3,3] CrI_3,[4,5] $CrGeTe_3$,[6,7] and $CrSiTe_3$[8,9]), antiferromagnetism (e.g., $MnBi_2Te_4$,[10] $MnP(S/Se)_3$,[11] and $CrCl_3$[12]), helimagnetism (e.g., $NiBr_2$[13] and NiI_2[14]), and frustrated magnetism (e.g., $RuCl_3$[15]).

Fe_3GeTe_2 is a 2D magnetic material that has been generating significant attention as it was the first vdW material found to be both magnetic and metallic. It also offers a significant step up in Curie temperature ($T_c \sim 225$ K) from previous magnetic vdW materials.[16−18] Much research has been directed toward tuning the magnetic properties of this material by layer thickness dependence studies,[19] varying the Fe content,[20] Co substitution,[21,22] and the investigation of the anomalous Hall effect,[23] planar topological Hall effect,[24] Kondo lattice physics,[25] anisotropy magnetostriction effect,[26] and ionic liquid voltage gating.[27] In bulk Fe_3GeTe_2, there have been some conflicting reports over whether the ground state of Fe_3GeTe_2 should be antiferromagnetic or ferromagnetic.[28−30]

In its stoichiometric form, there should be interlayer antiferromagnetism in Fe_3GeTe_2; however, Fe vacancies in this system, which correspond to more hole charge carriers, produce a ferromagnetic ground state.[30] This observation agrees with the majority of the literature, in which samples are frequently reported to be Fe-deficient and ferromagnetic.[20] It has also been suggested that an antiferromagnetic to ferromagnetic transition in Fe_3GeTe_2 can be induced by electron doping.[30]

In addition to the highly tunable nature of the magnetic properties of Fe_3GeTe_2, there have been several studies concentrating on skyrmions and the spin textures that have been observed in this material. Magnetic bubble-like formations were first observed in Fe_3GeTe_2 when a magnetic Ni tip of a scanning tunneling microscope (STM) was held close to a freshly cleaved surface of Fe_3GeTe_2.[31] Lorentz transmission electron microscopy (TEM) measurements further revealed magnetic bubble-like textures in Fe_3GeTe_2,

Received: June 14, 2021
Revised: September 16, 2021

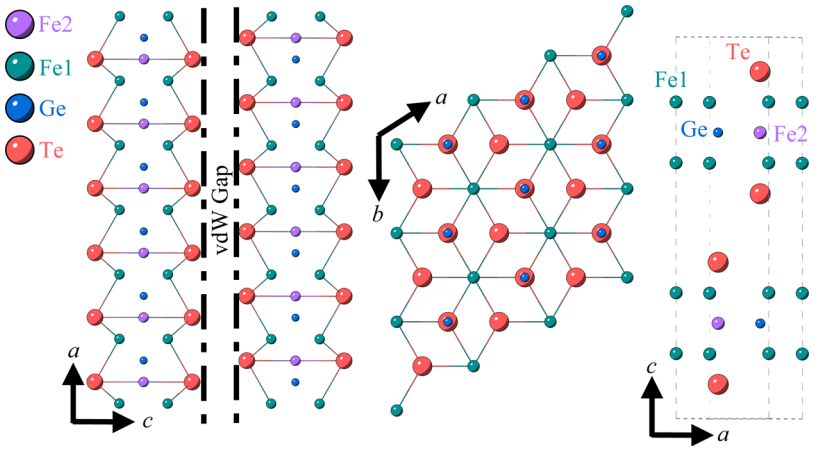

Figure 1. Crystal structure of Fe_3GeTe_2 along several crystallographic orientations. The vdW bonding is most easily observed when looking along the *ac* plane as indicated by the dashed-dotted lines between the Te layers. The hexagonal nature of the structure is clearly observable when looking perpendicular to the *ab* plane. The partial occupancy of Fe at the 2c (Fe2) site is found to be instrumental in determining the nature of the magnetic transition in Fe_3GeTe_2. The Fe atoms found on the 4c (Fe1) and 2c (Fe2) sites are shown in green and purple, respectively. The Te and Ge atoms are indicated in red and blue, respectively. The dashed lines indicate the unit cell of Fe_3GeTe_2.

which were claimed to be skyrmions.[32] These bubbles could be tuned in size with applied magnetic field. The presence of a topological Hall effect has recently been observed in Fe_3GeTe_2; this signal is frequently taken as the hallmark of skyrmions.[24,33] Since Fe_3GeTe_2 crystallizes in the centrosymmetric hexagonal space group $P6_3/mmc$ (No. 194) as shown in Figure 1, the mechanism for the stabilization of skyrmions in bulk Fe_3GeTe_2 is currently unclear. Skyrmion-like magnetic bubbles have only been observed in Fe_3GeTe_2 in a thin-film regime or at the interface of the material, as is the case for the STM study, where it is conceivable that inversion symmetry can be broken, leading to a Dzyaloshinskii−Moriya (DM) interaction.[34] The observation of Néel-type skyrmions at an oxide interface in Fe_3GeTe_2 gives further confirmation that the DM interaction is allowing the stabilization of skyrmions in this material.[35] Should skyrmions be realized in bulk Fe_3GeTe_2, the interactions stabilizing them cannot include the DM interaction due to the centrosymmetric nature of the crystal structure.

We have undertaken a detailed investigation into the dependence of the magnetic properties on the Fe content in the Fe_3GeTe_2 materials. We have synthesized both polycrystalline and single crystals of Fe_3GeTe_2 and Co-substituted materials, $Fe_{3-y}Co_yGeTe_2$ for y = 0.3, 0.6, 0.9, 1.2, and 1.5. Investigations of the structure and properties of the polycrystalline and single crystals produced have been undertaken using X-ray diffraction and magnetic measurement techniques. Composition analysis, including estimates of the Fe content in these materials, reveal a direct correlation with the observed magnetic transitions. We also find that an excess of Fe is necessary for the synthesis of Fe_3GeTe_2 to optimize the Fe content and therefore achieve the highest T_c.

EXPERIMENTAL DETAILS

Polycrystalline materials were synthesized by solid-state reaction. Single-crystal growths were carried out by either chemical vapor transport (CVT) or the flux method using Te flux. All of the sample preparation techniques are discussed in more detail in the following section. To determine the phase purity and crystal structure of the synthesized polycrystalline materials, powder X-ray diffraction was performed at room temperature using a Panalytical Empyrean diffractometer (Bragg−Brentano geometry) with a Cu $K_{\alpha1}$ and $K_{\alpha2}$ source and a solid-state PIXcel detector. Rietveld refinements were carried out on the observed diffraction patterns using the TOPAS academic v6.0 software suite.[36] The quality of the single crystals obtained was investigated by Laue X-ray imaging using a Photonic Science Laue camera.

The chemical composition was determined using a ZEISS GeminiSEM 500, which was used to perform energy-dispersive X-ray spectroscopy (EDX). The magnetic properties of both the single crystals and the polycrystalline materials were measured using a Quantum Design Magnetic Property Measurement System (MPMS) superconducting quantum interference device (SQUID) magnetometer. Measurements were made in the temperature range of 2−300 K in various applied magnetic fields in the zero-field-cooled (ZFC) and field-cooled (FC) modes.

MATERIAL SYNTHESIS

Polycrystalline Synthesis. Polycrystalline materials of Fe_3GeTe_2 and $Fe_{3-y}Co_yGeTe_2$ (y = 0.3, 0.6, 0.9, 1.2, 1.5) were synthesized by the solid-state reaction. Stoichiometric quantities of high-purity elements in powder form, Fe (STREM Chemicals, Inc., 99.99%), Co (Alfa Aesar, 99.998%), Ge (Acros Organics, 99.999%), and Te (Alfa Aesar, 99.99%) were ground together inside an argon-filled glovebox and transferred into quartz ampoules. The evacuated quartz ampoules were held at 675 °C for 10 days with heating/cooling rates of ca. 60−100 °C/h. The resulting gray/black powders were ground and investigated for phase formation.

Single-Crystal Growth. Two different techniques were employed to obtain single crystals of the various compositions listed: chemical vapor transport and the flux method using excess Te.

For the CVT process, growth was attempted using two different transport agents, I_2 and $TeCl_4$. Quantities of Fe, Ge, Co, and Te powders (see Table 1) along with 5 mg/cm^3 of the transport agent were sealed in quartz ampoules. The growth of crystals was carried out by holding the source and the sink ends of each tube at different temperatures in a two-zone furnace for 2 weeks, before cooling to room temperature. Several different temperature profiles were used, 750−675 °C for the hot end and 700−650 °C for the cold end. In some of the CVT growth processes, in addition to the platelets that have been identified as corresponding to the desired Fe_3GeTe_2 crystals, other needle-like and pyramidal-shaped structures

https://doi.org/10.1021/acs.cgd.1c00684
Cryst. Growth Des. XXXX, XXX, XXX−XXX

Table 1. Nominal Starting Compositions along with the Eventual Compositions Determined by EDX Analysis for Single Crystals of Fe−Ge−Te and Fe−Co−Ge−Te Grown by either CVT or the Flux Method

nominal composition	composition from EDX	growth technique
$Fe_{2.0}GeTe_4$	$Fe_{2.59}GeTe_{2.08}$	flux
$Fe_{3.0}GeTe_2$	$Fe_{2.63}GeTe_{1.98}$	CVT
$Fe_{3.0}GeTe_2$	$Fe_{2.73}GeTe_{2.03}$	CVT
$Fe_{3.0}GeTe_2$	$Fe_{2.84}GeTe_{2.04}$	CVT
$Fe_{3.0}GeTe_2$	$Fe_{2.96}GeTe_{2.18}$	CVT
$Fe_{3.25}GeTe_2$	$Fe_{3.00}GeTe_{2.17}$	CVT
$Fe_{2.00}Co_{0.60}GeTe_4$	$Fe_{1.88}Co_{0.90}GeTe_{2.18}$	flux
$Fe_{2.00}Co_{0.60}GeTe_4$	$Fe_{1.84}Co_{0.85}GeTe_{2.08}$	flux
$Fe_{2.10}Co_{0.90}GeTe_2$	$Fe_{1.60}Co_{1.10}GeTe_{1.76}$	CVT
$Fe_{2.10}Co_{0.90}GeTe_2$	$Fe_{1.65}Co_{0.99}GeTe_{1.74}$	CVT
$Fe_{2.25}Co_{0.75}GeTe_2$	$Fe_{1.58}Co_{1.27}GeTe_{2.16}$	CVT
$Fe_{2.25}Co_{0.75}GeTe_2$	$Fe_{1.67}Co_{1.08}GeTe_{1.96}$	CVT
$Fe_{2.25}Co_{0.75}GeTe_2$	$Fe_{2.74}Co_{0.05}GeTe_{2.00}$	CVT
$Fe_{2.25}Co_{0.75}GeTe_2$	$Fe_{2.78}Co_{0.06}GeTe_{1.96}$	CVT
$Fe_{2.70}Co_{0.30}GeTe_2$	$Fe_{2.44}Co_{0.48}GeTe_{2.11}$	CVT
$Fe_{2.70}Co_{0.30}GeTe_2$	$Fe_{2.47}Co_{0.44}GeTe_{2.08}$	CVT

corresponding to other phases of Fe−Ge−Te were also obtained. A photograph of a typical crystal platelet obtained from a CVT growth is shown in Figure 2a.

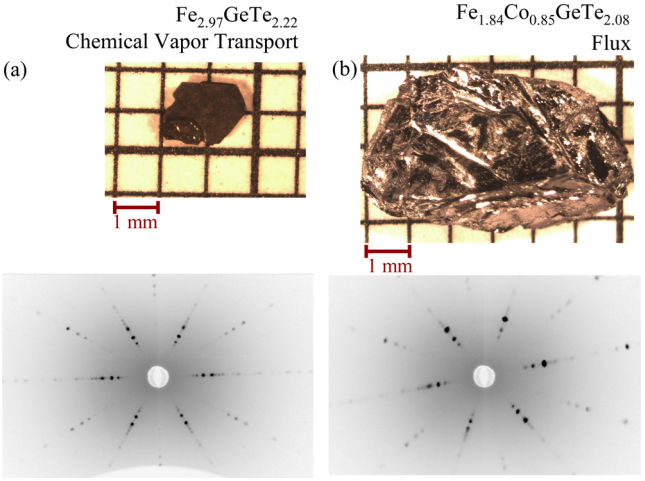

Figure 2. Typical as-grown crystal of (a) $Fe_{3.25}GeTe_2$ prepared using CVT and (b) $Fe_{3-y}Co_yGeTe_2$ grown by the flux method. The compositions of the single crystals are those estimated by EDX analysis. Below each picture is a corresponding Laue diffractogram displaying the sixfold symmetry expected observing along the *c* axis of the crystal.

For the crystal growth by the flux method, using excess Te (powder) as the flux, mixtures of varying nominal compositions (see Table 1) were used. The mixtures were placed in an alumina crucible, which was then sealed in a quartz ampoule under vacuum. To enable the capture of the crystals during a subsequent centrifuging process, a small amount of quartz wool was placed over the alumina crucible inside the ampoule. The tubes were heated to 1000 °C and cooled at the rate of 3 °C/h to 675 °C, at which temperature, the tubes were removed from the furnace and centrifuged to remove the excess Te flux.[20,32] An example of a crystal grown by the flux method is shown in Figure 2b.

In general, the thickness and size of the crystals grown by the flux method were found to be larger than those obtained by CVT. The average size of the CVT-grown crystals is 2 × 2 mm^2, while that obtained by the flux method is typically 7 × 5 mm^2.

RESULTS AND DISCUSSION

Laue Diffraction. X-ray back-reflection Laue patterns were taken on the crystals to check for crystalline quality. Typical Laue photographs of isolated platelets of Fe_3GeTe_2 and $Fe_{3-y}Co_yGeTe_2$, mounted with the *ab* plane perpendicular to the X-ray beam are shown in Figure 2a,b. They display the sixfold symmetry expected observing along the *c* axis of the crystals.

Powder X-ray Diffraction. Phase purity and structural analysis were carried out using powder X-ray diffraction on the polycrystalline materials synthesized. The diffraction patterns obtained could be indexed to the hexagonal space group $P6_3/mmc$ (No. 194). Figure 3 shows the observed diffraction

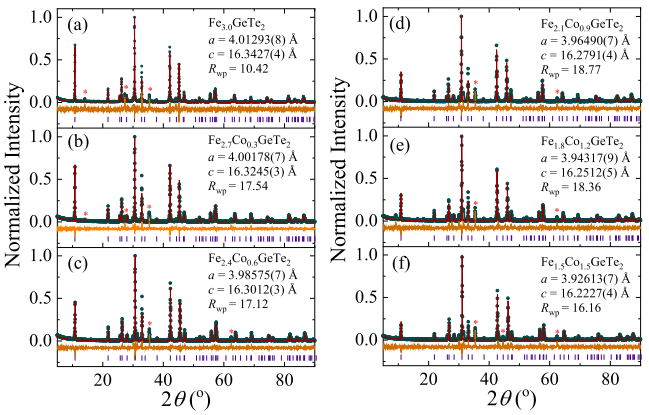

Figure 3. Room-temperature powder X-ray diffraction patterns of polycrystalline samples with the nominal compositions (a) $Fe_{3.0}GeTe_2$, (b) $Fe_{2.7}Co_{0.3}GeTe_2$, (c) $Fe_{2.4}Co_{0.6}GeTe_2$, (d) $Fe_{2.1}Co_{0.9}GeTe_2$, (e) $Fe_{1.8}Co_{1.2}GeTe_2$, and (f) $Fe_{1.5}Co_{1.5}GeTe_2$. Shown are the experimental profiles (green circles) and the Rietveld refinement (red solid line) made using the hexagonal $P6_3/mmc$ space group with the calculated difference (orange solid line). The purple bars indicate the expected positions of the Bragg peaks. The physical and crystallographic parameters obtained for $Fe_{3.0}GeTe_2$ are given in Table 2. Impurity peaks are denoted by a red asterisk.

patterns for the various nominal starting compositions of the Fe−Ge−Te and Fe−Co−Ge−Te powders and the Rietveld refinements of the observed patterns obtained using the TOPAS software suite. The typical physical and crystallographic parameters obtained for one of the compositions synthesized, Fe_3GeTe_2, are given in Table 2 along with the R_{wp} values indicating the quality of the fits. The lattice parameters obtained from the fits to the powder diffraction patterns are also shown in Figure 3. The lattice parameters obtained are largely in agreement with those reported for these materials.[16]

The variations in the lattice parameters in the Co-substituted powders can be seen to follow a clear trend by tracking the (103) and (006) diffraction peaks as shown in Figure 4. This gradual shift in the positions of the peaks indicates a decrease in both the *a* and *c* lattice parameters, as the level of Co substitution is increased in these materials.

The dependence of the lattice parameters on Fe composition in $Fe_{3-\delta}GeTe_2$ has been examined. We show

https://doi.org/10.1021/acs.cgd.1c00684
Cryst. Growth Des. XXXX, XXX, XXX−XXX

Table 2. Crystallographic Parameters Obtained from a Rietveld Refinement of the Powder X-ray Diffraction Pattern Collected at Room Temperature for a Polycrystalline Sample with a Nominal Composition Fe_3GeTe_2

nominal composition	Fe_3GeTe_2
refined composition	$Fe_{2.84}GeTe_2$
structure	hexagonal
space group	$P6_3/mmc$ (no. 194)
formula units/unit cell (Z)	2
lattice parameters	
a (Å)	4.0129(1)
c (Å)	16.3428(4)
V_{cell} (Å^3)	227.919(2)
ρ (g/cm^3)	7.0876(3)
R_{wp} (%)	10.42
R_{Bragg} (%)	2.401
GOF	2.77

atom	Wyckoff position	occupancy	x	y	z
Fe1	4e	1	0	0	0.6703(3)
Fe2	2c	0.839(8)	2/3	1/3	3/4
Ge1	2d	1	1/3	2/3	3/4
Te1	4f	1	2/3	1/3	0.58992(11)

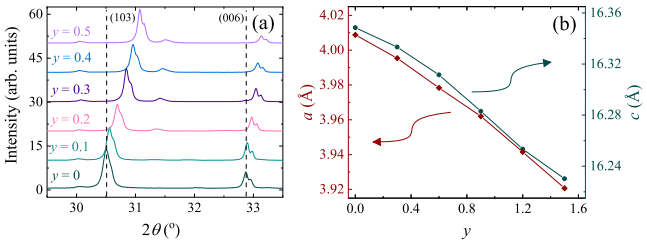

Figure 4. (a) Shift of the (103) and (006) diffraction peaks with increasing Co content y in $Fe_{3-y}Co_yGeTe_2$. The splitting of the peaks is due to the presence of Cu $K_{\alpha1}$ and $K_{\alpha2}$ radiation in the X-ray source. (b) Variation of the lattice parameters a (left axis, red diamonds) and c (right axis, green circles) with the Co content y in $Fe_{3-y}Co_yGeTe_2$.

that Fe deficiency results in a decrease in a, while c increases. We find that both the a and c lattice parameters decrease with increasing Co substitution at the Fe site, consistent with that reported earlier.[21] It was not possible to determine the actual occupancy levels of the Fe/Co in the Co-substituted samples using X-ray diffraction, due to the similar atomic numbers and hence X-ray scattering factors of the Fe and Co atoms. Therefore, the decrease observed in the lattice parameters can only be indirectly attributed to the preferential substitution of Co at the 2c (Fe2) sites.

X-ray diffraction patterns were also obtained on single-crystal platelets mounted with the ab plane parallel to the X-ray beam when the scattering angle is zero, to obtain a series of (00l) reflections. Figure 5 shows the diffraction patterns obtained from two different crystal platelets, exhibiting the (00l) reflections typical of the Fe_3GeTe_2 structure.

Energy-Dispersive X-ray Analysis. Composition analysis of the crystals obtained was carried out by EDX analysis. Estimates of the relative Fe, Co, Ge, and Te contents in the crystals are given in Table 1. Examples of the EDX spectra and scanning electron microscope images of two crystals are shown in Figure 6. The elemental stoichiometry at each numbered site and across the bulk is given in Table 3. The composition analysis reveals that the Fe content in the crystals is consistently lower than the nominal starting compositions for the various growths.

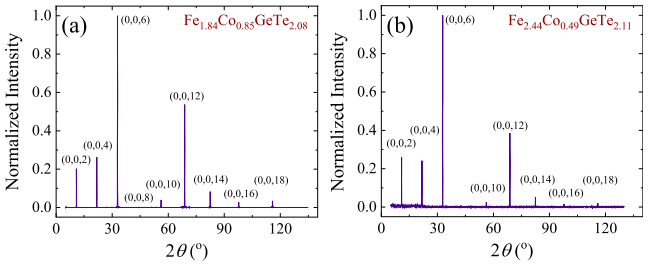

Figure 5. X-ray diffraction patterns obtained on single crystals with estimated compositions of (a) $Fe_{1.84}Co_{0.85}GeTe_{2.08}$ and (b) $Fe_{2.44}Co_{0.49}GeTe_{2.11}$. The platelets were mounted with the ab plane parallel to the X-ray beam when the scattering angle was zero and the (00l) reflections observed are shown.

Crystal growths of unsubstituted Fe_3GeTe_2 were attempted while varying the starting Fe content. For crystal growths starting with a nominal Fe content of 3.25, the resulting estimated Fe content in the crystals is close to 3. This indicates that an excess of Fe in the starting materials is necessary to ensure that a maximum occupancy of the Fe sites is achieved. For crystal growths starting with a particular Fe content, it was found that the Fe content in the resulting crystals varied considerably, providing crystals with a range of compositions. An indication of the typical range of final compositions for a nominal starting Fe content of 3.0 is given in the top half of Table 1. For the Co-substituted crystals obtained by both the flux method and CVT growths, the resulting composition of the crystals differed considerably from the nominal starting compositions. Each growth produced a number of crystals, which, when examined, showed varying Co content. This spread of Co levels estimated for a few typical crystals obtained from crystal growths with two starting Co substitution levels (y = 0.3 and 0.75) are shown in Table 1. These resulting compositions are further affirmed by the correlation with the T_c measured on these crystals through magnetic susceptibility measurements as discussed in the next section.

Magnetic Susceptibility versus Temperature. The Curie temperature, T_c, of a polycrystalline sample with a nominal composition Fe_3GeTe_2 was determined from the temperature-dependent dc magnetic susceptibility $\chi(T)$ as shown in Figure 7 and gave T_c = 223(1) K. This transition is not as sharp as that observed in the single crystals; however, the results are in agreement with previously reported magnetization data for polycrystalline Fe_3GeTe_2.[20]

Field-cooled-cooling dc magnetic susceptibility versus temperature curves for single crystals obtained from CVT with nominal Fe starting compositions of 3 and 3.25 are shown in Figure 8. The compositions given in the legend are estimated from EDX. The magnetic susceptibility confirms a ferromagnetic ordering in $Fe_{3-\delta}GeTe_2$ indicated by the sharp increase in T_c due to spontaneous magnetization at the transition temperature. Crystals from the various crystal growth experiments carried out have a range of Fe content, which is reflected in the range of T_c's they exhibit. Fe deficiency in $Fe_{3-\delta}GeTe_2$ leads to both a disorder and magnetic dilution, and therefore, the highest T_c is obtained when the composition of the resulting crystals is close to Fe_3GeTe_2. A rather striking linear dependence of the magnetic transition temperature over a range of Fe content in the Fe_3GeTe_2 crystals obtained is shown in Figure 8c. The

https://doi.org/10.1021/acs.cgd.1c00684
Cryst. Growth Des. XXXX, XXX, XXX−XXX

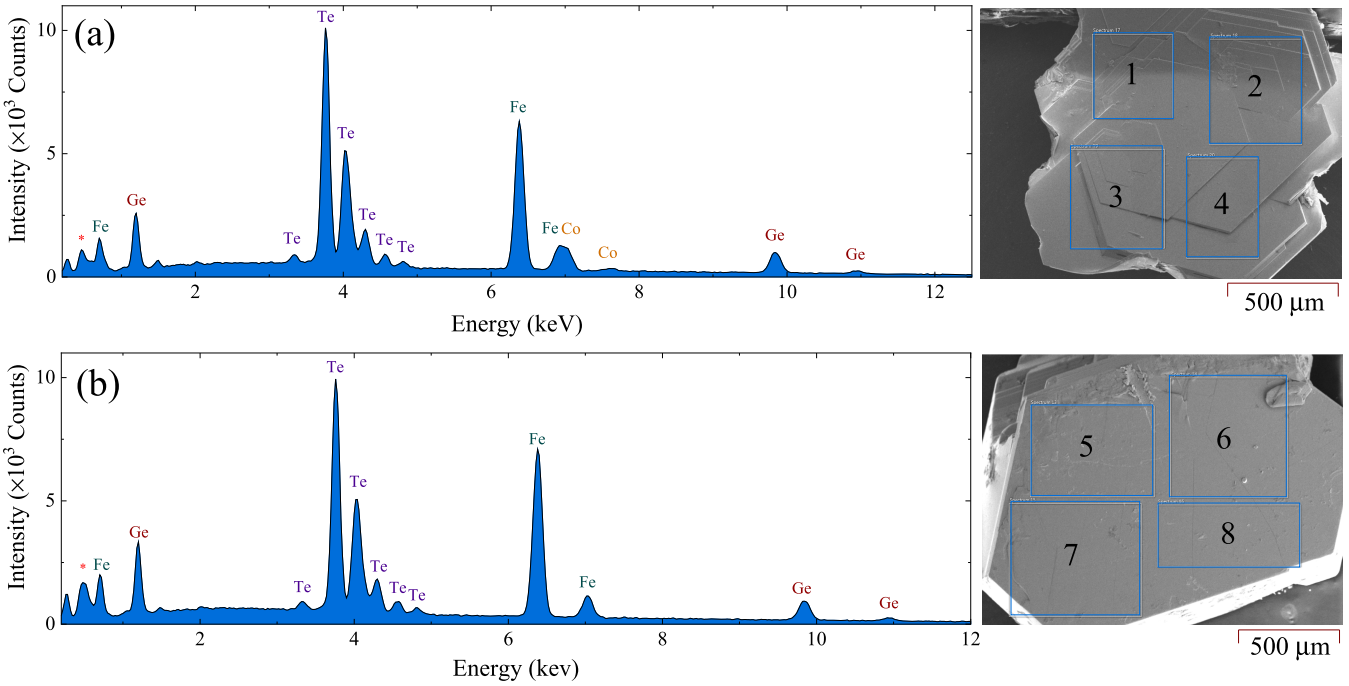

Figure 6. EDX spectra for single crystals with nominal starting compositions of (a) $Fe_{2.7}Co_{0.3}GeTe_2$ and (b) $Fe_{3.25}GeTe_2$, where the size and relative energies of the peaks indicate the elemental composition of the sample. The bulk stoichiometry was measured to be (a) $Fe_{2.44}Co_{0.486}GeTe_{2.11}$ and (b) $Fe_{2.97}GeTe_{2.22}$. Intensity peaks for each element are labeled. Oxygen peaks are indicated by a red asterisk. On the right is a scanning electron microscope image of the surface of each single crystal studied. EDX spectra were collected over the entire area of each crystal. The elemental stoichiometry at each numbered site and across the bulk is given in Table 3.

Table 3. Composition across Selected Sites of Single Crystals with the Nominal Starting Compositions $Fe_{2.7}Co_{0.3}GeTe_2$ and $Fe_{3.25}GeTe_2$ as Indicated in Figure 6 Determined from Energy-Dispersive X-ray Analysis

spectrum label	Fe (%)	Co (%)	Ge (%)	Te (%)
		$Fe_{2.7}Co_{0.3}GeTe_2$		
1	41.05(1)	7.76(1)	16.61(1)	34.58(1)
2	40.27(1)	8.16(1)	16.59(1)	34.99(1)
3	40.56(1)	7.93(1)	16.72(1)	34.79(1)
4	40.10(1)	8.31(1)	16.22(1)	35.37(1)
		$Fe_{3.25}GeTe_2$		
5	47.90(1)	0	16.16(1)	35.94(1)
6	47.44(1)	0	16.39(1)	36.17(1)
7	48.35(1)	0	15.61(1)	36.04(1)
8	48.13(1)	0	16.38(1)	35.49(1)

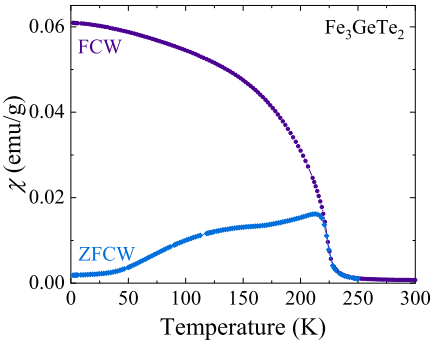

Figure 7. Zero-field-cooled warming (ZFCW) and field-cooled warming (FCW) dc magnetic susceptibility versus temperature for a polycrystalline sample with a nominal composition Fe_3GeTe_2 in an applied field of 100 Oe.

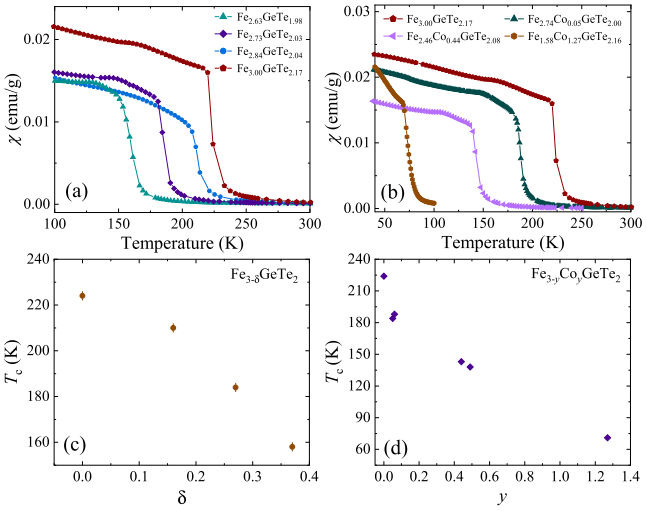

Figure 8. (a) Magnetic susceptibility as a function of temperature for several crystals of $Fe_{3-\delta}GeTe_2$ with differing levels of Fe content. Data were collected in the field-cooled cooling mode with H = 100 Oe applied along the c axis. (b) Magnetic susceptibility as a function of temperature for several crystals of $Fe_{3-y}Co_yGeTe_2$ with differing levels of Co content. Data were collected in zero-field-cooled warming mode in a field of 100 Oe applied along the c axis. (c) Transition temperature of $Fe_{3-\delta}GeTe_2$ as a function of Fe deficiency δ. (d) Transition temperature of $Fe_{3-y}Co_yGeTe_2$ as a function of Co content y.

magnetic susceptibility versus temperature behavior in Co-substituted Fe−Ge−Te is shown in Figure 8b. Again the compositions given in the legend are those estimated by EDX. The magnetic susceptibility of Fe_3GeTe_2 is included for comparison. The transition temperatures of the Co-substituted

https://doi.org/10.1021/acs.cgd.1c00684
Cryst. Growth Des. XXXX, XXX, XXX−XXX

Fe_3GeTe_2 are shown in Figure 8d. Ferromagnetism is preserved for all of the Co substitutions attempted here (up to y = 1.27), with an almost linear decrease in T_c with increasing Co levels.

SUMMARY AND CONCLUSIONS

The layered magnetic material, Fe_3GeTe_2, has been investigated in both polycrystalline and single-crystal forms. Polycrystalline powders of Fe_3GeTe_2 and $Fe_{3-y}Co_yGeTe_2$ with several nominal starting compositions and Co substitutions have been synthesized. The effect of varying the nominal starting Fe content on the resulting Fe compositions in the $Fe_{3-\delta}GeTe_2$ obtained has been studied. We have also produced high-quality single crystals with varying Co content ranging from y = 0 to 1.5 by both CVT and the flux method. The phase formation, composition analysis, and crystal structures have been investigated using EDX and both powder and single-crystal X-ray diffraction techniques. Our results demonstrate that CVT consistently produces Fe-deficient crystals when starting with the nominal stoichiometry of Fe_3GeTe_2, while starting with an increased Fe content results in crystals with Fe stoichiometry close to the desired Fe_3. With the crystal growth of the Co-substituted crystals by the flux method, starting with a fixed value of y was found to result in crystals exhibiting a range of Co substitutions. The fortuitous range of materials with varying levels of both Fe and Co content produced in this study has allowed us to investigate the dependence of the lattice parameters as well as the magnetic transition temperatures in these systems. The magnetic transition temperatures of all of the crystals synthesized have been measured, and we find a strong correlation of the transition temperature with the estimated Fe content, with compositions close to the optimum of three exhibiting the highest T_c. Similarly, the suppression of the magnetic transition temperature with Co substitution has been found. The systematic study of the structural and magnetic properties of these crystals is of great help in understanding the correlations between the synthesis and the structural and magnetic properties in this interesting magnetic material. Such a study is especially important as materials with T_c's close to room temperature are seen as being ideal for their applicability to device fabrication. Further studies probing the magnetic properties, especially in relation to their potential to exhibit skyrmions, are currently being explored on these crystals, for which they are ideal. Fe_3GeTe_2 continues to remain as one of the most interesting 2D magnetic materials with great promise for applications.

AUTHOR INFORMATION

Corresponding Authors

Daniel A. Mayoh − *Department of Physics, University of Warwick, Coventry CV4 7AL, U.K.*; orcid.org/0000-0002-7020-3263; Email: d.mayoh.1@warwick.ac.uk

Geetha Balakrishnan − *Department of Physics, University of Warwick, Coventry CV4 7AL, U.K.*; Email: g.balakrishnan@warwick.ac.uk

Authors

George D. A. Wood − *Department of Physics, University of Warwick, Coventry CV4 7AL, U.K.*

Samuel J. R. Holt − *Department of Physics, University of Warwick, Coventry CV4 7AL, U.K.*

Grady Beckett − *Department of Physics, University of Warwick, Coventry CV4 7AL, U.K.*

Emily J. L. Dekker − *Department of Physics, University of Warwick, Coventry CV4 7AL, U.K.*

Martin R. Lees − *Department of Physics, University of Warwick, Coventry CV4 7AL, U.K.*

Complete contact information is available at: https://pubs.acs.org/10.1021/acs.cgd.1c00684

Notes

The authors declare no competing financial interest.

ACKNOWLEDGMENTS

The authors acknowledge Tom Orton, Patrick Ruddy, and Daisy Ashworth for their technical support. They also thank David Walker for his assistance with the powder X-ray diffraction and Steve York for his assistance with the energy-dispersive X-ray spectroscopy measurements. This work was financially supported by two Engineering and Physical Sciences Research Council grants: EP/T005963/1 and the UK Skyrmion Programme Grant EP/N032128/1.

REFERENCES

(1) Mak, K. F.; Shan, J.; Ralph, D. C. Probing and controlling magnetic states in 2D layered magnetic materials. *Nat. Rev. Phys.* **2019**, *1*, 646−661.

(2) Burch, K. S.; Mandrus, D.; Park, J.-G. Magnetism in two-dimensional van der Waals materials. *Nature* **2018**, *563*, 47−52.

(3) Zhang, Z.; Shang, J.; Jiang, C.; Rasmita, A.; Gao, W.; Yu, T. Direct Photoluminescence Probing of Ferromagnetism in Monolayer Two-dimensional $CrBr_3$. *Nano Lett.* **2019**, *19*, 3138−3142.

(4) Li, T.; Jiang, S.; Sivadas, N.; WAng, Z.; Weber, D.; Goldberger, J. E.; Watanabe, K.; Taniguchi, T.; Fennie, C. J.; Mak, K. F.; Shan, J.; et al. Pressure-controlled interlayer magnetism in atomically thin CrI_3. *Nat. Mater.* **2019**, *18*, 1303−1308.

(5) Liu, Z.; et al. Observation of nonreciprocal magnetophonon effect in nonencapsulated few-layered CrI_3. *Sci. Adv.* **2020**, *6*, No. eabc7628.

(6) Carteaux, V.; Brunet, D.; Ouvard, G.; Andre, G. Crystallographic, magnetic and electronic structures of a new layered ferromagnetic compound $Cr_2Ge_2Te_6$. *J. Phys.: Condens. Matter* **1995**, *7*, 69−87.

(7) Han, M.-G.; Garlow, J. A.; Liu, Y.; Zhang, H.; Li, J.; DiMarzio, D.; Knight, M. W.; Petrovic, C.; Jariwala, D.; Zhu, Y. Topological Magnetic-Spin Textures in Two-Dimensional van der Waals $Cr_2Ge_2Te_6$. *Nano Lett.* **2019**, *19*, 7859−7865.

(8) Carteaux, V.; Ouvard, G.; Grenier, J. C.; Laligant, Y. Magnetic structure of the new layered ferromagnetic chromium hexatellurosilicate $Cr_2Ge_2Te_6$. *J. Magn. Magn. Mater.* **1991**, *94*, 127−133.

(9) Cai, W.; Sun, H.; Xia, W.; Wu, C.; Liu, Y.; Liu, H.; Gong, Y.; Yao, D.-X.; Guo, Y.; Wang, M. Pressure-induced superconductivity and structural transition in ferromagnetic $CrSiTe_3$. *Phys. Rev. B* **2020**, *102*, No. 144525.

(10) Deng, Y.; Yu, Y.; Shi, M. Z.; Guo, Z.; Xu, Z.; Wang, J.; Chen, X. H.; Zhang, Y. Quantum anomalous Hall effect in intrinsic magnetic topological insulator $MnBi_2Te_4$. *Science* **2020**, *367*, 895−900.

(11) Susner, M. A.; Chyasnavichyus, M.; McGuire, M. A.; Ganesh, P.; Maksymovych, P. Metal Thio- and Selenophosphates as Multifunctional van der Waals Layered Materials. *Adv. Mater.* **2017**, *29*, No. 1602852.

(12) Kuhlow, B. Magnetic Ordering in $CrCl_3$ at the Phase Transition. *Phys. Status Solidi A* **1982**, *72*, 161−168.

(13) Tokunaga, Y.; Okuyama, D.; Kurumaji, T.; Arima, T.; Nakao, H.; Murakami, Y.; Taguchi, Y.; Tokura, Y. Multiferroicity in $NiBr_2$ with long-wavelength cycloidal spin structure on a triangular lattice. *Phys. Rev. B* **2011**, *84*, No. 060406.

(14) Kurumaji, T.; Seki, S.; Ishiwata, S.; Murakawa, H.; Kaneko, Y.; Tokura, Y. Magnetoelectric responses induced by domain rearrangement and spin structural change in triangular-lattice helimagnets NiI_2 and CoI_2. *Phys. Rev. B* **2013**, *87*, No. 014429.
(15) Kim, H.-S.; V, V. S.; Catuneanu, A.; Kee, H.-Y. Kitaev magnetism in honeycomb $RuCl_3$ with intermediate spin-orbit coupling. *Phys. Rev. B* **2015**, *91*, No. 241110.
(16) Deiseroth, H.-J.; Aleksandrov, K.; Reiner, C.; Kienle, L.; Kremer, R. K. Fe_3GeTe_2 and Ni_3GeTe_2 − Two New Layered Transition-Metal Compounds: Crystal Structures, HRTEM Investigations, and Magnetic and Electrical Properties. *Eur. J. Inorg. Chem.* **2006**, *2006*, 1561−1567.
(17) Chen, B.; Yang, J.; Wang, H.; Imai, M.; Ohta, H.; Michioka, C.; Yoshimura, K.; Fang, M. Magnetic Properties of Layered Itinerant Electron Ferromagnet Fe_3GeTe_2. *J. Phys. Soc. Jpn.* **2013**, *82*, No. 124711.
(18) Li, Q.; et al. Patterning-Induced Ferromagnetism of Fe_3GeTe_2 van der Waals Materials beyond Room Temperature. *Nano Lett.* **2018**, *18*, 5974−5980.
(19) Fei, Z.; Huang, B.; Malinowski, P.; Wang, W.; Song, T.; Sanchez, J.; Yao, W.; Xiao, D.; Zhu, X.; May, A. F.; Wu, W.; Cobden, D. H.; Chu, J.-H.; Xu, X. Two-Dimensional Itinerant Ferromagnetism in Atomically Thin Fe_3GeTe_2. *Nat. Mater.* **2018**, *17*, 778−782.
(20) May, A. F.; Calder, S.; Cantoni, C.; Cao, H.; McGuire, M. A. Magnetic structure and phase stability of the van der Waals bonded ferromagnet $Fe_{3-x}GeTe_2$. *Phys. Rev. B* **2016**, *93*, No. 014411.
(21) Tian, C.-K.; Wang, C.; Ji, W.; Wang, J.-C.; Xia, T.-L.; Wang, L.; Liu, J.-J.; Zhang, H.-X.; Cheng, P. Domain wall pinning and hard magnetic phase in Co-doped bulk single crystalline Fe_3GeTe_2. *Phys. Rev. B* **2019**, *99*, No. 184428.
(22) Hwang, I.; Coak, M. J.; Lee, N.; Ko, D.-S.; Oh, Y.; Jeon, I.; Son, S.; Zhang, K.; Kim, J.; Park, J.-G. Hard ferromagnetic van-der-Waals metal $(Fe,Co)_3GeTe_2$: a new platform for the study of low-dimensional magnetic quantum criticality. *J. Phys.: Condens. Matter* **2019**, *31*, No. 50LT01.
(23) Kim, K.; et al. Large anomalous Hall current induced by topological nodal lines in a ferromagnetic van der Waals semimetal. *Nat. Mater.* **2018**, *17*, 794−799.
(24) You, Y.; Gong, Y.; Li, H.; Li, Z.; Zhu, M.; Tang, J.; Liu, E.; Yao, Y.; Xu, G.; Xu, F.; Wang, W. Angular dependence of the topological Hall effect in the uniaxial van der Waals ferromagnet Fe_3GeTe_2. *Phys. Rev. B* **2019**, *100*, No. 134441.
(25) Zhang, Y.; Lu, H.; Zhu, X.; Tan, S.; Feng, W.; Liu, Q.; Zhang, W.; Chen, Q.; Liu, Y.; Luo, X.; Xie, D.; Luo, L.; Zhang, Z.; Lai, X. Emergence of Kondo lattice behavior in a van der Waals itinerant ferromagnet, Fe_3GeTe_2. *Sci. Adv.* **2018**, *4*, No. eaao6791.
(26) Zhuang, H. L.; Kent, P. R. C.; Hennig, R. G. Strong anisotropy and magnetostriction in the two-dimensional Stoner ferromagnet Fe_3GeTe_2. *Phys. Rev. B* **2016**, *93*, No. 134407.
(27) Deng, Y.; Yu, Y.; Song, Y.; Zhang, J.; Wang, N. Z.; Sun, Z.; Yi, Y.; Wu, Y. Z.; Wu, S.; Zhu, J.; et al. Gate-tunable room-temperature ferromagnetism in two-dimensional Fe_3GeTe_2. *Nature* **2018**, *563*, 94−99.
(28) Yi, J.; Zhuang, H.; Zou, Q.; Wu, Z.; Cao, G.; Tang, S.; Calder, S. A.; Kent, P. R. C.; Mandrus, D.; Gai, Z. Competing antiferromagnetism in a quasi-2D itinerant ferromagnet: Fe_3GeTe_2. *2D Mater.* **2017**, *4*, No. 011005.
(29) Kong, X.; Nguyen, G. D.; Lee, J.; Lee, C.; Calder, S.; May, A. F.; Gai, Z.; Li, A.-P.; Liang, L.; Berlijn, T. Interlayer magnetism in $Fe_{3-x}GeTe_2$. *Phys. Rev. Mater.* **2020**, *4*, No. 094403.
(30) Jang, S. W.; Yoon, H.; Jeong, M. Y.; Ryee, S.; Kim, H.-S.; Han, M. J. Origin of ferromagnetism and the effect of doping on Fe_3GeTe_2. *Nanoscale* **2020**, *12*, 13501−13506.
(31) Nguyen, G. D.; Lee, J.; Berlijn, T.; Zou, Q.; Hus, S. M.; Park, J.; Gai, Z.; Lee, C.; Li, A.-P. Visualization and Manipulation of Magnetic Domains in the Quasi-Two-Dimensional Material Fe_3GeTe_2. *Phys. Rev. B* **2018**, *97*, No. 014425.
(32) Ding, B.; Li, Z.; Xu, G.; Li, H.; Hou, Z.; Liu, E.; Xi, X.; Xu, F.; Yao, Y.; Wang, W. Observation of Magnetic Skyrmion Bubbles in a van der Waals Ferromagnet Fe_3GeTe_2. *Nano Lett.* **2020**, *20*, 868−873.
(33) Chowdhury, R. R.; DuttaGupta, S.; Patra, C.; Sharma, S.; Fukami, S.; Ohno, H.; Singh, R. P. Unconventional Hall effect and it variation with Co-doping in van der Waals Fe_3GeTe_2. *Sci. Rep.* **2021**, *11*, No. 14121.
(34) Dzyaloshinsky, I. A thermodynamic theory of "weak" ferromagnetism of antiferromagnetics. *J. Phys. Chem. Solids* **1958**, *4*, 241−255.
(35) Park, T.-E.; Peng, L.; Liang, J.; Hallal, A.; Yasin, F. S.; Zhang, X.; Song, K. M.; Kim, S. J.; Kim, K.; Weigand, M.; et al. Néel-type skyrmions and their current-induced motion in van der Waals ferromagnet-based heterostructures. *Phys. Rev. B* **2021**, *103*, No. 104410.
(36) Coelho, A. A. *TOPAS* and *TOPAS-Academic*: an optimization program integrating computer algebra and crystallographic objects written in C++. *J. Appl. Crystallogr.* **2018**, *51*, 210−218.

https://doi.org/10.1021/acs.cgd.1c00684
Cryst. Growth Des. XXXX, XXX, XXX−XXX